



Cite this: *Dalton Trans.*, 2014, **43**, 14992

Novel 4'-functionalized 4,4''-dicarboxyterpyridine ligands for ruthenium complexes: near-IR sensitization in dye sensitized solar cells†

Ganesh Koyyada,^{a,b} Vinayak Botla,^a Suresh Thogiti,^a Guohua Wu,^c Jingzhe Li,^c Xiaqin Fang,^c Fantai Kong,^{*c} Songyuan Dai,^{c,d} Niveditha Surukonti,^a Bhanuprakash Kotamarthi^{a,b} and Chandrasekharam Malapaka^{*a,b}

Novel ruthenium complexes (**MC113–MC117**), obtained by modifying the terpyridine ligand of the black dye (**N749**), have been evaluated as sensitizers for dye sensitized solar cells (DSSCs). The modification is carried out by attaching selected chromophores, with varying electron donating strength, covalently to the central ring of the ligand. The complexes, compared to the parent dye, show red shifted absorption covering visible and near IR regions and higher molar extinction coefficients. We report in this work synthesis of a series of these ruthenium complexes with chromophores such as *tert*-butyl phenyl, triphenylamine, bithiophene, phenoxazine and phenothiazine. Detailed experimental characterization using optical, electrochemical and photovoltaic techniques has been carried out and complemented by density functional theory studies. The fill factors (ff) obtained for these dyes are larger than those of the parent black dye. In spite of these superior properties, the dyes show only moderate to good power conversion efficiencies. The possible reasons for this have been investigated and discussed.

Received 30th May 2014,
Accepted 24th June 2014
DOI: 10.1039/c4dt01598c

www.rsc.org/dalton

Introduction

Dye sensitized solar cells (DSSCs) have attracted increasing attention as promising alternatives to conventional silicon based solar cells due to their low cost and ease of fabrication.^{1,2} The optimum efficiency of a DSSC device depends upon several parameters and particularly the structure of the sensitizer plays a major role. The ground and excited state energy levels of the dye should be well matched with the highest occupied molecular orbital (HOMO) level of the redox mediator and the conduction band of the semiconductor, respectively, in order to facilitate easy regeneration of the sensitizer and facile electron injection onto TiO₂.^{3–11} Among a large variety of dyes investigated for DSSC application,^{11–30} Ru-sensitizers^{11–17} have attracted more attention because of their low lying metal–ligand charge transfer (MLCT) transition that

extends into the red and near-infrared region of the solar spectrum, contributing to very high efficiencies of **N3**,¹¹ **N719**¹² and **N749**.¹³ In this context, much attention has been devoted to enhance the performance of DSSCs by engineering sensitizers. For example, ancillary ligands of the bipyridyl ruthenium complexes have been modified for tuning the photophysical properties of the sensitizers leaving the dicarboxy bipyridine for performing its duty of grafting the sensitizer onto the TiO₂ for effective electronic communication.^{31–42} In contrast, the structural variation of ruthenium-terpyridyl complexes warrants the presence of an anchoring group as well as the tunable chromophores on the same terpyridyl ligand and are comparatively less addressed because of the synthetic challenges involved. Ruthenium complexes with an electron donating group on the terminal ring of the dicarboxy terpyridines have been reported,^{43–45} while terpyridine ligands carrying the two carboxy groups on the terminal rings and the electron donating group on the middle ring have not been reported for DSSC applications.

The application of the black dye (**N749**) was successfully explored as a base-dye along with small organic molecules as co-sensitizers achieving the highest certified record efficiency.⁴⁶ The broad absorption properties of the terpyridyl ruthenium complexes offer a large space for structural modification to further improve the DSSC performance. Such modifications can extend the absorption of a sensitizer further into

^aNetwork of Institutes for Solar Energy, CSIR-Indian Institute of Chemical Technology, I&PC Division, Uppal Road, Tarnaka, Hyderabad-500 607, India.
E-mail: chandra@iict.res.in; Fax: +914027193186

^bAcademy of Scientific and Innovative Research, CSIR-IICT, India

^cKey Laboratory of Novel Thin Film Solar Cells, Institute of Plasma Physics, Chinese Academy of Sciences, Hefei, 230031, P. R. China

^dState Key Laboratory of Alternate Electrical Power System with Renewable Energy Sources, North China Electric Power University, Beijing, 102206, P. R. China

†Electronic supplementary information (ESI) available. See DOI: 10.1039/c4dt01598c

the near infrared region. While not all such modifications lead to highly efficient sensitizers, many of these give us an opportunity to understand in detail the structure and property relationship. These studies also give us a deep insight into more fundamental issues like charge transfer, polarization, binding, *etc.* Keeping this in view, we in this work have modified the terpyridine ring by substituting chromophores covalently on the central ring while retaining the anchoring groups on the terminal rings to create novel ligands that can form complexes with the Ru metal. These new ruthenium terpyridyl sensitizers are shown as **MC113–MC117** in Fig. S1 (ESI[†]).

The functionalization of the central ring in these complexes has been systematically studied by attaching chromophores with different electron donating strength. In **MC113** the chromophore is a *tert*-butyl phenyl group which is shown to have a moderately electron donating moiety.^{47,48} In **MC114**, the triarylamine group, a widely used chromophore in electro and optical materials, is incorporated owing to its strong electron donating and transporting capability and the propeller starburst molecular shape.^{48,49} Hexyl bithiophene, which has been used as the chromophore in **MC115**, is expected to increase the solubility and red shift the absorption peak, apart from increasing the molar extinction coefficient of the sensitizer.^{50,51} Diheteroanthracenes (phenoxazine and phenothiazines) are heterocyclic compounds with electron-rich oxygen/sulfur and nitrogen heteroatoms, and these molecules are non-planar with a butterfly conformation in the ground state, which can impede the molecular aggregation and the formation of intermolecular excimers.^{52–55} Phenoxazine and phenothiazines are also potential hole transport materials in organic devices, presenting unique electronic and optical properties. Hence these moieties were selected as chromophores in **MC116** and **MC117**.

Detailed experimental characterization of the new ruthenium complexes **MC113–MC117** has been carried out using optical, electrochemical and photovoltaic techniques while the standard quantum chemical software has been employed for DFT studies. A structure–property relationship between the substituted terpyridyl group in the ruthenium complexes and the efficiency of the DSSC device has been systematically studied.

Results and discussion

Synthesis

We introduced different electron donor groups at the central pyridine (4'-position) of terpyridine by the Krohnke method.^{56,58} The synthetic route for **MC113–MC117** is shown in Scheme 1. Isonicotinic acid was used as the starting material. The ethylisonicotinate derivative **6** was synthesized, according to a previously published procedure, in 90% yield.⁵⁷ Compound **6** was subjected to acylation using paraldehyde and CF₃COOH in acetonitrile medium under reflux for 4 h to give 2-acetyl isonicotinate (**7**) in 61% yield. The intermediate

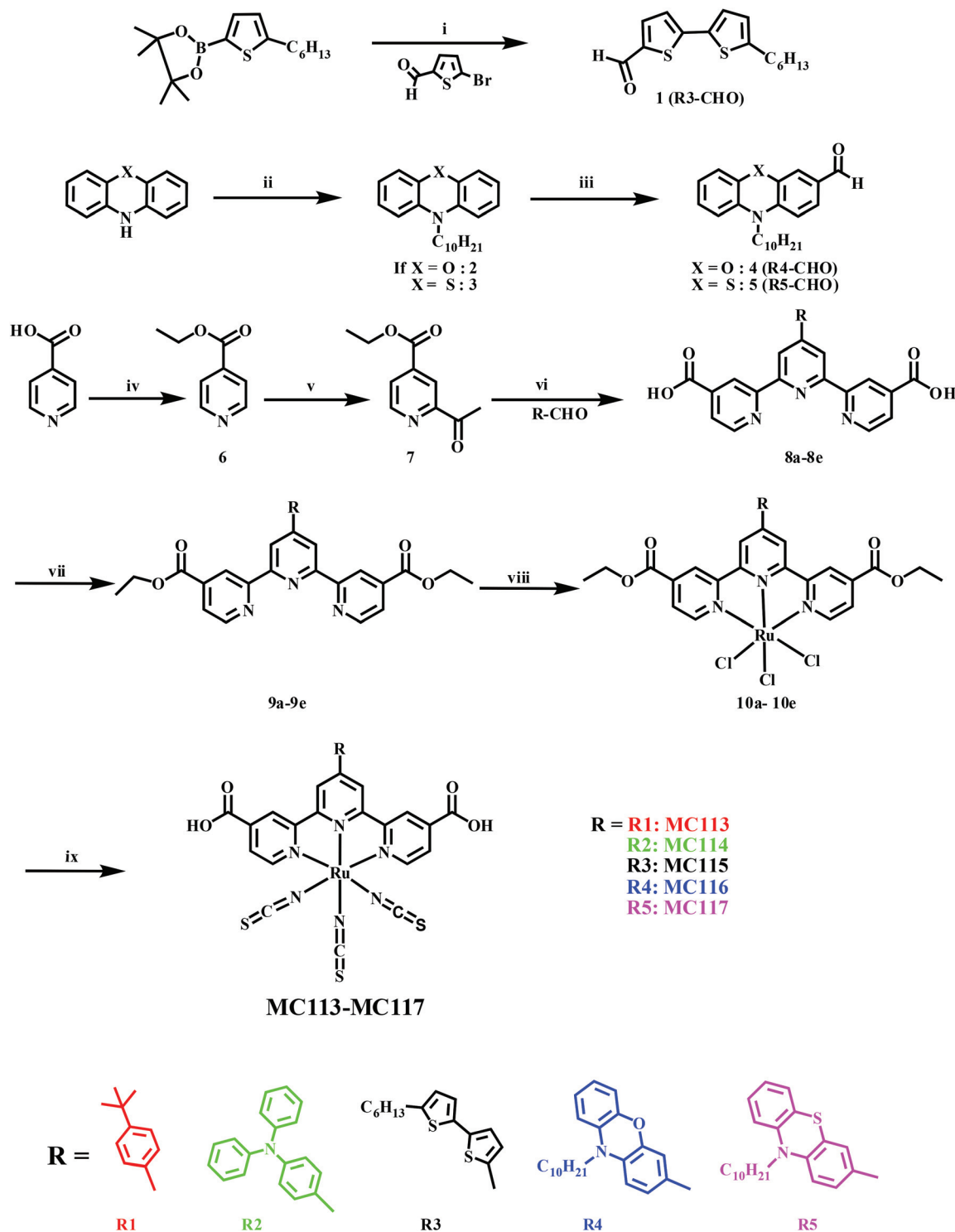
R3-aldehyde (**1**) was synthesized using 5-hexylthiophene-2-boronic acid pinacol ester and 5-bromothiophene-2-carbaldehyde under Suzuki reaction conditions. The aldehydes **4** and **5** were synthesized by N-alkylation followed by the Vilsmeier–Haack formylation on phenoxazine and phenothiazine respectively. The commercially available aldehyde partners (R1-CHO and R2-CHO) and the aldehydes **1**, **4–5** were further reacted with **7** in the presence of sodium hydroxide and ammonia in methanol affording 40–50% yields of the corresponding 4'-functionalized 4,4''-dicarboxyterpyridine (**8**). The terpyridine ligands (**8a–e**) on complexation with RuCl₃·3H₂O, followed by treatment with NH₄NCS results in the formation of diester, which upon hydrolysis using triethylamine afforded the desired ruthenium complexes (**MC113–MC117**) in 39–47% yield. The new complexes were characterised by nuclear magnetic resonance spectroscopy (NMR) and electrospray-ionization mass spectra (ESI-MS).

Geometries

Knowledge of the geometry is important to understand the properties and also the effect of substitution. The optimized ground state geometries of the complexes **MC113–MC117** are shown in Fig. S2 (ESI[†]). Bulky alkyl groups of the ancillary ligands are replaced with methyl groups so as to minimize the computational complexity without compromising the quantitative picture. The optimized geometries reveal that the basic Ru[3 + 3] skeleton of **MC113–MC117** is like that of an octahedron. The carboxylic acid groups and the pyridines of all the complexes are in the same plane. The optimized geometry parameters are tabulated in Table 1 and Table S1 (ESI[†]). It has been observed that there is not much variation of the geometry with regard to both bond lengths and bond angles on substitution with different chromophores.

Molecular orbitals

Analysis of the molecular orbitals, obtained using computational methods, would be helpful to understand some fundamental properties of the molecules, like the nature of charge transfer of the electronic transitions. Additionally the HOMO and the LUMO energies can also be compared to the values obtained by differential pulse voltammetry (DPV) experiments to obtain a complementary picture of the frontier orbitals. The molecular orbitals obtained at the M06/LANL2DZ level of theory along with the percentage contributions of the individual groups are shown in detail in Fig. S3 (ESI[†]) and the important ones (mainly HOMO, LUMO and LUMO+1) in Fig. 1. The molecular orbital pictures indicate that the HOMOs of the molecules **MC113–MC115**, **MC117** are distributed on the Ru atom (~40%), NCS (~40%), and terpyridine ligands (~20%), while HOMO of **MC116** is distributed evenly on all the three groups, *viz.*, Ru (32%), NCS (30%), and terpyridine (38%). HOMO–1 of **MC113–MC117** has similar contribution from all three groups, *viz.*, Ru (~43%), NCS (~45%), and terpyridine (~12%). HOMO–2 of **MC116** is mainly located on terpyridine (76%). HOMO–3 of **MC113** is mainly located on NCS (100%), and for the molecules **MC114**, **MC115**, **MC117** it



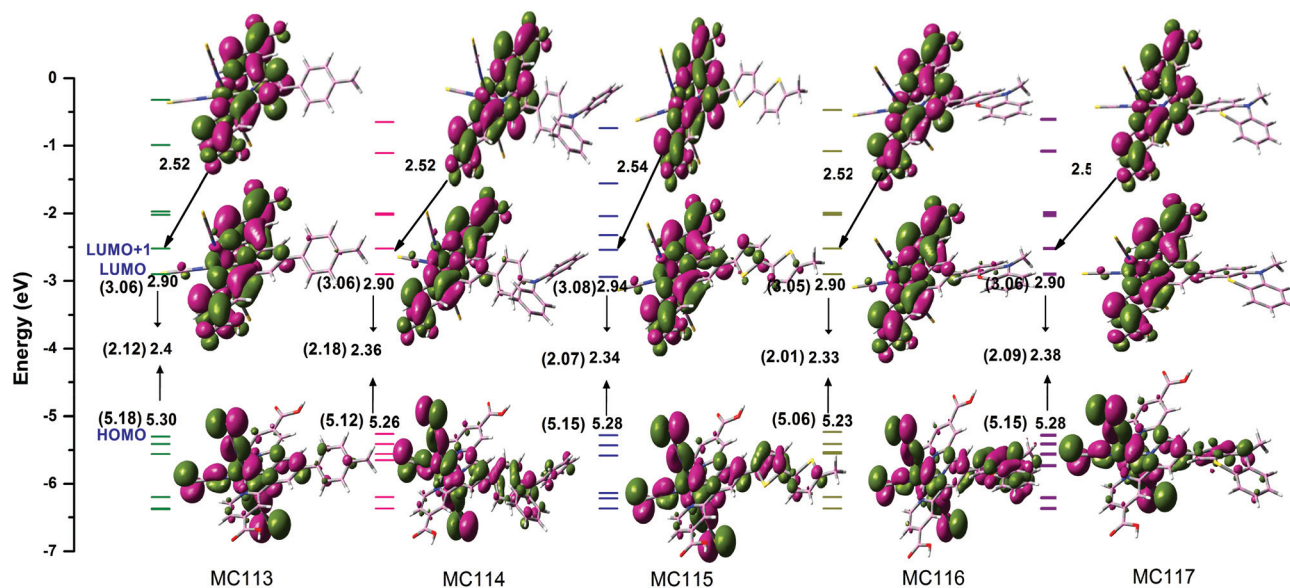
Scheme 1 (i) Pd(PPh₃)₄ NaCO₃, DME, 80 °C 6 h; (ii) NaH, DMF, 1-bromodecane, RT, 12 h; (iii) DMF, POCl₃, 1,2-dichloroethane reflux, 12 h; (iv) CH₃CH₂OH, conc. H₂SO₄, 6 h, reflux; (v) paraldehyde, *t*-BuOOH, FeSO₄·7H₂O, CF₃COOH, CH₃CN, reflux, 4 h; (vi) NaOH, NH₄OH (aq), CH₃OH; (vii) EtOH, conc. H₂SO₄, reflux, 6 h; (viii) RuCl₃·3H₂O, EtOH/CHCl₃, reflux under dark, 4 h; (ix) (a) DMF reflux, 4 h, (b) NH₄NCS, reflux, 2 h, (c) TEA, H₂O, reflux, 48 h.

is delocalized on terpyridine (>70%), NCS (<30%), and Ru atom (<5%). LUMO as well as LUMO+1 and LUMO+3 of all the molecules have major contributions from terpyridine ligands (>90%).

It is also clear from these pictures that the HOMO is slightly delocalized on the chromophore attached to the central ring in all the molecules. Inspecting the antibonding orbitals we note that in LUMO and LUMO+1 the contribution from the chrom-

Table 1 Optimized geometry parameters of MC113–MC117 calculated using the PBE0 functional, in gas phase

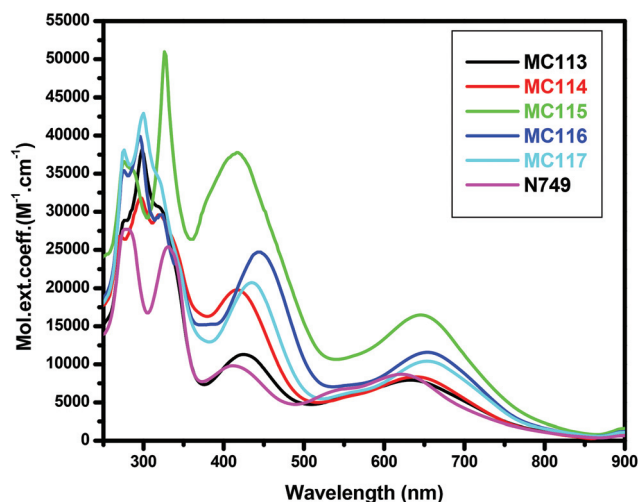
MC113	MC114	MC115	MC116	MC117
Bond lengths (Å)				
Ru ₁ –N ₉				
2.035	2.035	2.035	2.035	2.035
Ru ₁ –N ₁₀				
1.932	1.932	1.929	1.930	1.932
Ru ₁ –N ₁₁				
2.035	2.035	2.035	2.034	2.034
Ru ₁ –N ₁₂				
2.047	2.047	2.045	2.041	2.042
Ru ₁ –N ₁₃				
2.022	2.022	2.019	2.022	2.022
Ru ₁ –N ₁₄				
2.022	2.022	2.019	2.021	2.021

**Fig. 1** HOMO, LUMO orbital pictures at M06/LANL2DZ level of MC113–MC117 and respective HOMO–LUMO gaps calculated at M06/LANL2DZ level of theory in DMF solvent. In parenthesis B3LYP/LANL2DZ calculated values are given.

phore is drastically reduced, thus indicating that if the excited state transition involves HOMO to LUMO or LUMO+1, then this transition would involve charge transfer from the chromophore to the central part of the terpyridine ligand.

Optical properties

The UV-Vis absorption spectra obtained for MC113–MC117 in DMF solvent is shown in Fig. 2 and relevant data summarized in Table 2. It is seen that all the molecules have an absorption in the range 250–900 nm. Compared to the N749 dye the new sensitizers show red shifted broad absorption covering visible and near-IR regions with higher molar extinction coefficients. The bands in the range 250–450 nm can be broadly attributed to the ligand centred π – π^* electronic transition and/or metal to ligand charge transition (MLCT). The bands corresponding to the longer wavelength (λ_{\max}) at 620–655 nm can be broadly attributed to the MLCT from the occupied 4d orbitals of ruthenium to the lowest unoccupied π^* orbitals of the terpyridine ligand.¹³ The λ_{\max} of MC113–MC117 in the low-energy region spans absorption range from 632 nm to 654 nm and is a result of chemical tuning of the complexes by structural design. The λ_{\max} bands of all the five sensitizers are red shifted around 10–30 nm relative to that of N749 (620 nm). The absorption

**Fig. 2** Absorption spectra of MC113–MC117 and N749 in DMF solution.

wavelength order follows MC113 (632 nm) < MC114 (638 nm) < MC115 (646 nm) < MC116 (654 nm) ~MC117 (654 nm), which is in line with the increasing conjugation length of the 4'-functionalized terpyridine ligands. The molar extinction coefficient

Table 2 Optical, electrochemical and photovoltaic data of sensitizers MC113–MC117

Dye	λ_{\max} ($\epsilon \times 10^4 \text{ M}^{-1} \text{ cm}^{-1}$) ^a [nm]	E_{oxd} ^b [V]	E_{0-0} ^c [eV]	E_{oxd}^* ^d [V]	V_{oc} ^e [V]	J_{sc} ^f [mA cm ⁻²]	ff ^g	η^h (%)
MC113	632 (0.7886)	0.67	1.75	-1.08	0.64	8.28	0.677	3.59
MC114	638 (0.8495)	0.66	1.65	-0.99	0.61	4.66	0.731	2.08
MC115	646 (1.6476)	0.67	1.61	-0.94	0.60	6.16	0.722	2.65
MC116	654 (1.1380)	0.64	1.64	-0.99	0.67	5.94	0.689	2.72
MC117	654 (1.0452)	0.67	1.62	-0.95	0.68	3.31	0.706	1.59
N749	620 (0.6884)				0.66	15.41	0.637	6.51

^a Absorption spectra were recorded in DMF solution. ^b Oxidation potentials were measured by DPV. ^c The bandgap, E_{0-0} , was derived from the intersection of the absorption and emission spectra. ^d E_{oxd}^* was calculated by subtracting E_{0-0} from E_{oxd} . ^e Open-circuit voltage. ^f Current density. ^g Fill factor. ^h Photoelectric conversion efficiency.

(ϵ) for the MLCT band of these ruthenium dyes are in the order MC115 ($16\,476 \text{ M}^{-1} \text{ cm}^{-1}$) > MC116 ($11\,637 \text{ M}^{-1} \text{ cm}^{-1}$) > MC117 ($10\,502 \text{ M}^{-1} \text{ cm}^{-1}$) > MC114 ($8335 \text{ M}^{-1} \text{ cm}^{-1}$) > MC113 ($7794 \text{ M}^{-1} \text{ cm}^{-1}$), which are comparable and higher than that of N749 ($8930 \text{ M}^{-1} \text{ cm}^{-1}$). Thus, these results indicate that extension of π -conjugation at the 4'-position of the terpyridyl ligand can lower the MLCT energy and also increase the absorption intensity and the effect is clearly seen in the case of MC115 absorption spectra with a bithiophene chromophore on the central ring ($\epsilon_{\max} = 16\,476 \text{ M}^{-1} \text{ cm}^{-1}$). In the case of tricyclic isomers (phenothiazine and phenoxazine), phenoxazine based MC116 showed a higher extinction coefficient compared to phenathiazine based MC117. This could be attributed to strong electron donating nature. The bathochromic shift and hyperchromic effects of the absorption in these new sensitizers indicate that in addition to e-donating character, the extension of conjugation at the 4'-position of the terpyridyl ligand through the incorporation of an aromatic segment is beneficial to the light-harvesting ability of the sensitizer.

TDDFT calculations were carried out to analyze the photo physical behaviour of these complexes and also for understanding the transitions in terms of molecular orbitals. The normalized plots of simulated and experimental UV-Vis spectra of MC113–MC117 are given in Fig. S4 (ESI†). The summarized data of important allowed transitions within the range of 450–850 nm in comparison with experimental λ_{\max} are given in Table S2 (ESI†). The results are in good agreement with experimental UV-Vis spectra. The most intense singlet transitions of MC113–MC117 in this range are shown. In MC113 it is dominant from HOMO to LUMO+1 (89%) at 657 nm, with oscillator strength, $f = 0.1274$. In MC114, it is from HOMO to LUMO+1 (95%) at 662 nm, with $f = 0.1227$. In MC115, it is from HOMO to LUMO+1 (89%) at 666 nm with $f = 0.1231$. In MC116, it is from HOMO to LUMO+1 (80%) at 665 nm with $f = 0.1231$, and for MC117 it is from HOMO to LUMO+1 (87%) at 660 nm with $f = 0.1238$. All these observations suggest that this transition is dominated by metal to terpyridine ligand and additionally it is also strengthened by the small charge transfer transition from the chromophore to the terpyridine ligand.

In general, the charge transfer in the molecules under study is dominant from their HOMO and HOMO–1 comprising largely of the Ru(II) atom and the NCS ligand, and partly

from HOMO–3, which is mainly distributed on ancillary part of the terpyridine ligand to LUMO, LUMO+1, LUMO+3, which are located mainly on the terpyridine ligand. From the orbital pictures, it can be inferred that the main allowed charge transfer transitions in the molecules are of metal–ligand (MLCT) and ligand–ligand (LLCT) as also inferred from the experimental data. The band gap, E_{0-0} , obtained from the intersection of the absorption and emission spectra is also shown in Table 2.

Redox properties

The differential pulse voltammetry measurements were carried out to obtain the oxidation potentials of the new sensitizers. The main aim is to obtain a picture of the availability of adequate driving energy for dye regeneration to occur and also the excited state oxidation potentials. The oxidation potentials of the Ru^{III/II} couple are calculated to be 0.67, 0.66, 0.67, 0.64 and 0.67 V (vs. the normal hydrogen electrode (NHE)) for MC113, MC114, MC115, MC116 and MC117, respectively (Fig. 3a and Table 2). This potential is sufficiently more positive than that of the Γ/I_3^- redox couple ($\sim 0.4 \text{ V}$ vs. NHE) and provides enough driving force for efficient dye regeneration.^{59–64} Excited state oxidation potentials must be sufficiently more negative than the TiO₂ conduction band for efficient electron injection. The excited-state oxidation potentials (E_{ox}^*) of MC113, MC114, MC115, MC116 and MC117 calculated from $E_{\text{HOMO}} - E_{0-0}$, are -1.08, -0.99, -0.94, -0.99 and -0.95 V vs. NHE, respectively. The E_{ox}^* values here are more negative than the conduction band edge of TiO₂ (-0.5 V vs. NHE) ensuring an efficient electron injection process from the excited state of the dyes into the TiO₂ electrode (Fig. 3b).^{65–69}

Thermogravimetric analysis

Thermogravimetric analysis was performed to evaluate the thermal stability of ruthenium sensitizers. The measurements were carried out in a TGA/SDTA 851 °C Thermal system (mettler Toledo, Switzerland) at a heating rate of $10 \text{ }^\circ\text{C min}^{-1}$ in the temperature range 25–600 °C under a N₂ atmosphere (flow rate, 30 mL min^{-1}). Film samples ranging from 1 to 7 mg were placed in the sample pan and heated. During the heating period the weight loss was recorded as a function of temperature. The incorporation of different electron donating groups (shown in Scheme 1, Fig. S1†) at the 4'-position of the

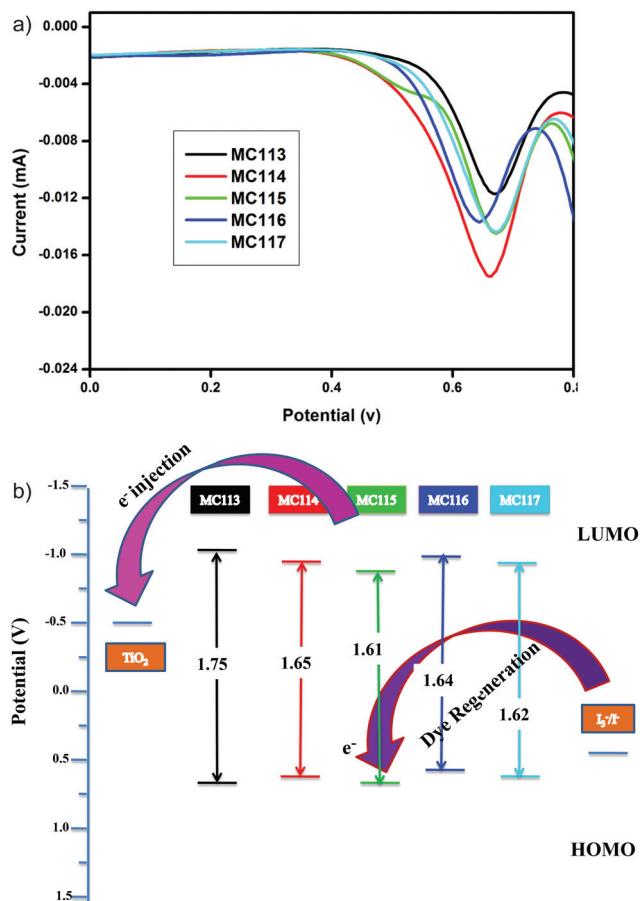


Fig. 3 (a) Oxidative differential pulse voltammetry of MC113–MC117. (b) The schematic energy levels of MC113–MC117 based on absorption and electrochemical data.

terpyridine ligand makes the dye more hydrophobic and increases the thermal stability. According to the thermogram (Fig. 4) MC113 and MC116 are more stable than all other sensitizers. Percentage of conversion of the sensitizers (MC113–MC117) at 600 °C are recorded as 10.82%, 41.94%, 33.83%,

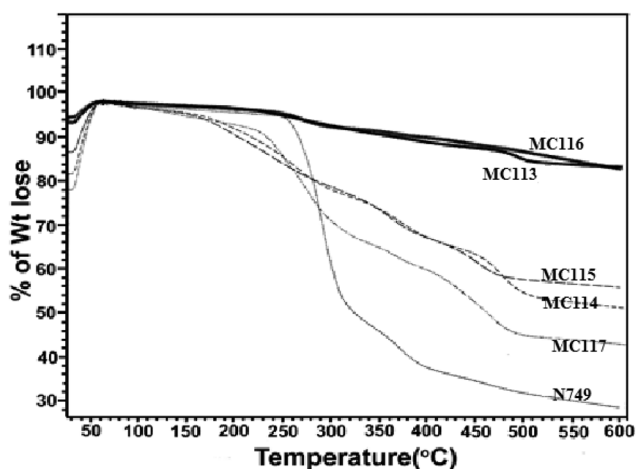


Fig. 4 Thermograms of the sensitizers MC113–MC117 relative to N749.

10.25%, 49.32%, respectively, and under similar conditions black dye recorded 64.57%.

Photovoltaic properties

The photovoltaic performance of the new sensitizers MC113–MC117 in DSSCs was tested by constructing the 0.25 cm² active area TiO₂ electrodes using a thermally stable electrolyte composed of 0.5 M 1,2-dimethyl-3-propylimidazole iodide (DMPPI), 0.05 M I₂ and 0.1 M LiI in acetonitrile. Fig. 5 shows the incident photon-to-current conversion efficiency (IPCE) as a function of excitation wavelength for DSSCs based on MC113–MC117, compared with N749. Notably, the IPCE of MC113 is the highest as compared to the other dyes reaching 34% at 590 nm, while it decreases to 18% at 590 nm, 20% at 590 nm, 24% at 590 nm and 15% at 540 nm for MC114, MC115, MC116 and MC117, respectively.

The lower IPCE values observed for MC113–MC117 when compared with N749 might be attributed to the steric constraints associated with the 4'-substitution units on the terpyridine resulting in the loss of co-planarity and conjugation while anchored on TiO₂. Further bulkiness of these 4'-substitutions might have prevented the effective grafting onto the TiO₂ surface slowing down the electron injection. Generally, it is known from the equation $IPCE = (1240 \times J_{sc})100/(\lambda \times P_{in})$ (in %) that the IPCE value is closely related to J_{sc} at a specific wavelength and a fixed input power (P_{in}). The IPCE values of the devices constructed from the new complexes are in the range of 310–750 nm and roughly follow the order of the J_{sc} values observed (MC113 > MC115 > MC116 > MC114 > MC117).

The J_{sc} , V_{oc} and ff of the DSSCs were measured under standard global AM 1.5 solar light (100 mW cm⁻²). The current–voltage (J – V) curves for DSSCs based on MC113–MC117 are shown (Fig. 6) and the detailed device performance data are listed in Table 2. The J_{sc} values of the solar cells for MC113–MC117 are 8.28, 4.66, 6.16, 5.94 and 3.31 mA cm⁻², respecti-

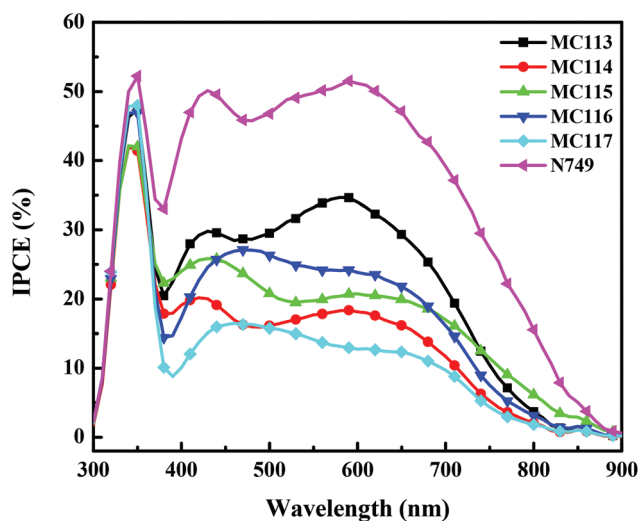


Fig. 5 Photocurrent action (IPCE) curves of the TiO₂ electrodes sensitized by MC113–MC117 and standard N749.

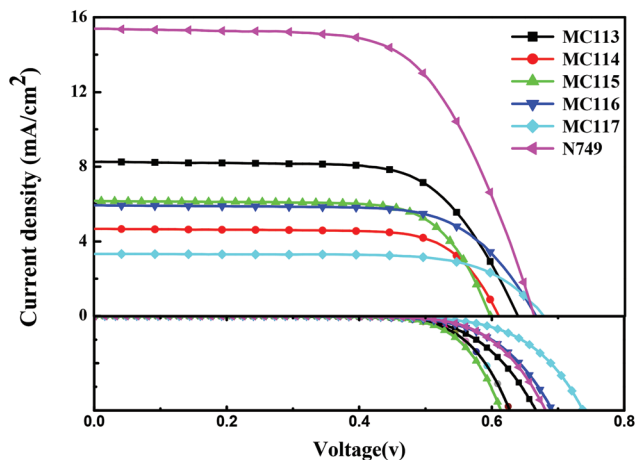


Fig. 6 Photocurrent–voltage (J – V) curves for the DSSCs based on MC113–MC117 and standard N749.

vely. The high J_{sc} observed for the MC113 is attributed to its high IPCE value in the range of 400–650 nm. It is obvious that the dark current of MC113–MC117 dyes is increased in the order of MC117 < MC116 < N749 < MC113 < MC114 < MC115 under the same bias leading to a consequent increase of recombination rate between the injected electrons and I_3^- in electrolytes, which causes a consequent decrease in V_{oc} values. An interesting point is that all these dyes show larger fill factors. The larger fill factors of the novel compounds MC113–MC117 are assumed to be arising from stronger intermolecular interactions suggesting better pathways for charge carriers to the electrodes. In addition this may be also attributed to the lower series resistances compared with N749 dye. The power conversion efficiencies (η) of MC113, MC114, MC115, MC116 and MC117 sensitized solar cells are moderate at 3.59%, 2.08%, 2.65%, 2.72% and 1.59%, respectively (*vs.* 6.51% for N749 under the same device-fabrication process and measuring conditions). The dye with the moderate electron donating group (MC113) exhibited a better photovoltaic performance with power conversion efficiency (η) of 3.59% than the other four dyes because of the increase in the J_{sc} value. The lower η is largely due to the lower J_{sc} of the sensitizers as compared to N749 that is associated with their lesser IPCE.

Electrochemical impedance spectroscopy

Electrochemical impedance spectroscopy (EIS) was performed in the dark under a bias of -0.60 V to characterize the charge transfer resistances of the cells with a frequency range of 50 mHz to 1000 kHz. The Nyquist plots for MC113–MC117 and N749 dye sensitized solar cells are shown in Fig. 7. It is observed that there are two semicircles in the Nyquist plots. The first smaller semicircle at higher frequency represents the charge transfer resistances at the Pt/electrolyte interface and the second larger one at lower frequency indicates charge recombination resistance at the TiO_2 /dye/electrolyte interface. It is obvious that the recombination resistance (R_{ct}) obtained from the Z-view software and the inset model at the TiO_2 /dye/

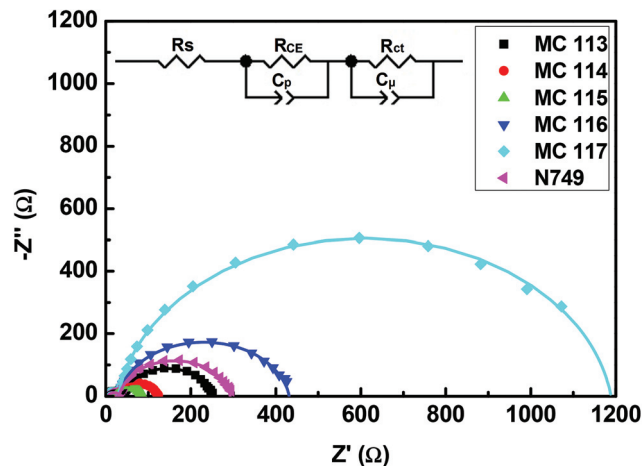


Fig. 7 EIS Nyquist plots for DSSCs based on MC113–MC117 sensitizers and the N749 dye (measured under dark conditions with an external potential of -0.60 V. The inset shows the equivalent circuit).

electrolyte interface is decreased in the order of MC117 (1159 Ω) > MC116 (402 Ω) > N749 (261 Ω) > MC113 (208 Ω) > MC114 (115 Ω) > MC115 (69 Ω), which indicates that the recombination reaction rate of the injected electron with the I_3^- in the electrolyte is increased in the order of MC117 < MC116 < N749 < MC113 < MC114 < MC115 in the dark. The simulated electron lifetime (τ_e) could be estimated by $\tau_e = R_{ct} \times C_{\mu}$. The corresponding τ_e values for the DSSCs based on MC113–MC117 and N749 dyes are 115 ms, 60 ms, 39 ms, 229 ms, 615 ms and 128 ms, respectively. The order of the above lifetime values is consistent with that of the R_{ct} and V_{oc} . Therefore, the enhanced electron lifetime may be the intrinsic reason for the higher V_{oc} values of the DSSCs based on MC117 and MC116 compared to that for N749.

Conclusions

Replacement of the carboxy group with a chromophore on the central ring of the terpyridine ligand in the ruthenium complex gives rise to enhanced absorption and higher molar absorption coefficient compared to N749. The novel, structurally modified ruthenium complexes also show better thermal stability. On the other hand when sensitized on the TiO_2 surface, there is a drop in the efficiency of the test cells which is resulting from lower IPCE values. This is probably due to the slowdown of electron injection capacity of the sensitizer, as the bulky substitution on the central ring of the terpyridine ligand may be hindering proper grafting of carboxylic groups on the TiO_2 . Most interestingly the fill factors of all the new sensitizers are higher compared to the parent N749 dye and are assumed to be arising from stronger intermolecular interactions suggesting better pathways for charge carriers to the electrodes. The experimental results complimented with DFT studies provided insights into the structure–property relationship. The exact reasons for the higher ff values and moderate efficiencies are under further investigation.

Experimental section

The starting materials phenothiazine, phenoxazine, isonicotinic acid, bromodecane, 4-tertiary butyl benzaldehyde (R1-CHO), 4-(diphenylamino) benzaldehyde (R2-aldehyde) and 5-hexyl-2-thiopheneboronic acid pinacol ester were purchased from Sigma Aldrich. The solvents were purified by a standard procedure and purged with nitrogen before use. All other chemicals used in this work were of analytical grade and were used without further purification, and all reactions were performed under an argon atmosphere. Chromatographic separations were carried out on silica gel (60–120 mesh). ^1H NMR and ^{13}C NMR spectra were recorded on an Avance 300 MHz spectrometer using tetramethylsilane (TMS) as an internal standard. Mass spectra were recorded on a Shimadzu model LCMS-2010EV system that was equipped with an electrospray ionization (ESI) probe. Absorption spectra were recorded on a Shimadzu ultraviolet-visible light (UV-vis) spectrometer. Electrochemical data were recorded using an Autolab potentiostat/Galvanostat PGSTAT30. The DPV curves were obtained from a three electrode cell in 0.1 M Bu_4NPF_6 , N,N -dimethylformamide solution at a scan rate of 100 mV s^{-1} , Pt wire as a counter electrode and an Ag/AgCl reference electrode and calibrated with ferrocene. Emission spectra were recorded on a J. Y. Horiba model Fluorolog3 fluorescence spectrometer.

Synthesis of 5'-hexyl-[2,2'-bithiophene]-5-carbaldehyde (1)

A 50 mL two neck round bottom flask was charged with hexylthiopheneboronic acid pinacol ester (0.511 mL, 1.7 mmol), $\text{Pd}(\text{PPh}_3)_4$ (0.196 g, 0.17 mmol), dimethoxy ethane (8 mL) and 2 M aqueous sodium carbonate (2 mL), then the tube was purged with argon gas. Under an inert atmosphere, 5-bromo-2-thiophenecarboxaldehyde (0.261 mL, 2.04 mmol) was added as a neat liquid. The tube was sealed and refluxed for 12 h at $90\text{ }^\circ\text{C}$ with vigorous stirring. The organic layers were extracted three times with EtOAc. The combined organic fractions were washed with brine and dried over Na_2SO_4 . The solvent was removed under reduced pressure and the residue purified by silica gel column chromatography using petroleum ether-ethylacetate (8/2; v/v) as the eluent to give the product as a yellow powder (0.457 g, 70%). ^1H NMR (300 MHz, CDCl_3 , δ in ppm): 9.83 (s, 1H), 7.64 (d, 1H), 7.17 (dd, 2H), 6.74 (d, 1H), 2.81 (t, 2H), 1.68 (m, 2H), 1.38 (m, 2H), 1.32 (m, 4H), 0.89 (t, 3H). ^{13}C NMR: 182.4, 148.6, 140.9, 137.4, 133.3, 126.0, 125.4, 123.3, 31.4, 30.2, 28.6, 22.5, 14.0. ESI-MS ($\text{C}_{15}\text{H}_{18}\text{OS}_2$): calcd 278.08, found: 279 ($\text{M} + \text{H}$) $^+$.

Synthesis of 10-decyl-10H-phenoxazine (2)

A 100 mL round bottom flask was charged with phenoxazine (2.00 g, 10.928 mmol), NaH (0.314 g, 13.114 mmol) and 30 mL of DMF. The mixture was stirred for 30 min and 1-bromodecane (2.70 mL, 13.114 mmol) was then added. The mixture was stirred overnight at room temperature. The reaction mixture was quenched with ice water (400 mL) and extracted three times with ethylacetate. The combined organic fractions were washed with brine and dried over Na_2SO_4 . The solvent was

removed under reduced pressure and the residue was purified by silica gel column chromatography using *n*-hexane-ethylacetate (9/1; v/v) as the eluent to give a viscous liquid (2.89 g, 82%). ^1H NMR (300 MHz, CDCl_3 , δ in ppm): 6.76 (t, 3H), 6.60 (m, 3H), 6.44 (m, 2H), 3.4 (t, 2H), 1.64 (m, 2H), 1.5 (m, 2H), 1.3 (m, 12H), 0.88 (t, 3H). ^{13}C NMR: 143.4, 139.2, 118.3, 117.5, 114.1, 48.5, 29.2, 28.1, 27.3, 22.7, 14.1. ESI-MS ($\text{C}_{22}\text{H}_{29}\text{NO}$): calcd 323.22, found: 324 ($\text{M} + \text{H}$) $^+$.

10-Decyl-10H-phenothiazine (3)

Compound 3 was synthesized by following the procedure described for 2 from phenothiazine (2.00 g 10.050 mmol), NaH (0.289 g, 12.060 mmol) and 1-bromodecane (3 mL, 12.060 mmol) and the product was obtained as a viscous liquid (2.75 g, 81%). ^1H NMR (300 MHz, CDCl_3 , δ in ppm): 7.13 (m, 4H), 6.8 (m, 3H), 3.84 (t, 2H), 1.78 (m, 2H), 1.4 (m, 2H), 1.2 (s, 12H), 0.87 (t, 3H). ^{13}C NMR: 145.2, 127.3, 127.0, 124.8, 122.2, 115.3, 47.3, 31.8, 29.49, 29.44, 29.2, 22.6, 14. ESI-MS ($\text{C}_{22}\text{H}_{29}\text{NS}$): calcd 339.20, found: 340 ($\text{M} + \text{H}$) $^+$.

Synthesis of 10-decyl-10H-phenoxazine-3-carbaldehyde (4)

To a solution of 10-decyl-10H-phenoxazine (2) (0.800 g, 2.476 mmol) and dry DMF (0.228 mL, 2.972 mmol) in 1,2-dichloroethane (DCE) (10 mL) kept at $0\text{ }^\circ\text{C}$ (ice water bath), POCl_3 (0.277 mL, 2.972 mmol) was added slowly. After the addition was complete the mixture was heated overnight at reflux. The reaction mixture was quenched with water and extracted three times with chloroform. The combined organic fractions were washed with brine and dried over Na_2SO_4 . The solvent was removed under reduced pressure and the residue was purified by silica gel column chromatography using petroleum ether-ethylacetate (8/2; v/v) as the eluent to give yellow powder (0.608 g, 70%). ^1H NMR (300 MHz, CDCl_3 , δ in ppm): 9.63 (s, 1H), 7.27–7.23 (m, 1H), 7.4 (m, 1H), 6.79–6.59 (m, 2H), 6.48–6.44 (m, 2H), 3.5 (t, 2H), 1.6 (m, 2H), 1.3 (m, 2H), 1.2 (s, 12H), 0.8 (t, 3H). ^{13}C NMR: 189.6, 145.0, 144.5, 139.2, 131.3, 129.7, 128.7, 123.8, 122.4, 115.6, 114.1, 112.0, 110.3, 44.2, 31.8, 29.5, 29.3, 26.8, 24.9, 22.6, 14.0. ESI-MS ($\text{C}_{23}\text{H}_{29}\text{NO}_2$): calcd 351.48, found: 352 ($\text{M} + \text{H}$) $^+$.

10-Decyl-10H-phenothiazine-3-carbaldehyde (5)

Compound 5 was synthesised by following the procedure described for 4 starting from 3 (0.8 g, 2.359 mmol), DMF (0.218 mL, 2.831 mmol), and POCl_3 (0.264 mL, 2.831 mmol) and the product was obtained as a yellow liquid (0.606 g, 72%). ^1H NMR (300 MHz, CDCl_3 , δ in ppm): 9.78 (s, 1H), 7.65–7.62 (dd, 1H), 7.58–7.57 (d, 1H), 7.19–7.09 (m, 2H), 6.98–6.93 (m, 1H), 6.90–6.86 (m, 2H), 3.8 (t, 2H), 1.85–1.75 (m, 2H), 1.43 (m, 2H), 1.23 (s, 12H), 0.87 (t, 3H). ^{13}C NMR: 187.2, 146.1, 144.5, 129.5, 128.2, 126.7, 125.4, 121.3, 117.2, 115.6, 114.2, 43.4, 30.7, 29.3, 29.1, 28.5, 22.3, 14.1. ESI-MS (m/z): 368 ($\text{M} + \text{H}$) $^+$.

Synthesis of ethyl 2-acetyl isonicotinate (7)

To a stirred solution of paraldehyde (47 g, 331.1 mmol) and ethyl isonicotinate (10 g, 66.2 mmol) in acetonitrile (140 mL)

at ambient temperature, FeSO₄·7H₂O (0.312 mg, 1.12 mmol), trifluoroacetic acid (7.49 g, 67.5 mmol) and 70% *t*-BuOOH (11.9 g, 132.4 mmol) were added and the mixture was refluxed for 4 h. The solvent was removed under reduced pressure and the residue was taken up in a saturated sodium carbonate aqueous solution (50 mL). The aqueous layer was extracted with toluene (3 × 75 mL). The combined organic fractions were dried (Na₂SO₄), filtered and the solvent was removed under reduced pressure. The residue was then purified by bulb-to-bulb distillation, giving 4.77 g (61%) of pure 7 as white crystals (mp = 56 °C). ¹H NMR (300 MHz, CDCl₃, δ in ppm): 1.25 (t, 3H), 2.76 (s, 3H), 4.44 (q, 2H), 8.40 (dd, 1H), 8.55 (s, 1H), 8.84 (d, 1H); ¹³C NMR (CDCl₃): δ ppm: 25.9, 62.1, 120.9, 126.1, 138.9, 149.8, 154.5, 164.6, 199.4; ESI-MS (C₂₃H₂₉NOS): calcd 367.20, found: 368 (M + H)⁺.

General procedure for the synthesis of 4'-substituted 4,4''-dicarboxyterpyridine (8a–8e)

A round bottomed flask was charged with ethyl 2-acetylisonicotinate (1.0 mmol) and aldehyde (0.5 mmol) in 120 mL methanol and to it was then added sodium hydroxide (3.0 mmol) and 25% aqueous ammonia (30 mL, 2.2 mol). The mixture was heated to reflux for 20 h. The resulting suspension was cooled to r.t. The precipitate obtained was collected by filtration and subsequently dissolved in hot water. After the solution cooled to r.t., hydrochloric acid (37%) was added until pH < 3. The precipitate was collected by filtration and was subjected to esterification without further purification.

General procedure for the synthesis of 4'-substituted 4,4''-dicarboxyterpyridine esters (9)

A suspension of 4'-functionalized, 4,4''-dicarboxy-2,2':6',2''-terpyridine (3.12 mmol) in methanol (absolute, 150 mL) and sulphuric acid (1 mL) was refluxed for 3 days. After cooling to room temperature, the precipitated white crystals were filtered and washed with methanol and ether.

Dimethyl 4'-(4-(*tert*-butyl)phenyl)-[2,2':6',2''-terpyridine]-4,4''-dicarboxylate (9a)

Yield (0.345 g, 65%), ¹H NMR (300 MHz, CDCl₃, δ in ppm): 9.15 (d, 2H), 8.42 (s, 2H), 8 (d, 2H), 7.76 (d, 2H), 7.4 (d, 2H), 3.3 (s, 6H), 1.3 (s, 9H). ¹³C NMR: 165.8, 157.3, 155.3, 152.4, 150.2, 149.8, 138.4, 135.1, 126.9, 125.9, 122.8, 120.7, 119.3, 52.7, 34.7, 31.2; ESI-MS (C₂₇H₂₃N₃O₄): calcd 481.20, found: 482 (M + H)⁺, 504 (M + Na)⁺.

Dimethyl 4'-(4-(diphenylamino)phenyl)-[2,2':6',2''-terpyridine]-4,4''-dicarboxylate (9b)

Yield (0.356 g, 68%) ¹H NMR (300 MHz, CDCl₃, δ in ppm): 9.17 (s, 2H), 8.86 (d, 2H), 8.7 (s, 2H), 7.9 (d, 2H), 7.7 (d, 2H), 7.3 (m, 4H), 7.1 (m, 6H), 7.08 (t, 2H); ¹³C NMR: 165.8, 157.3, 155.2, 149.8, 148.9, 147.2, 138.4, 131.2, 129.3, 129.0, 128.0, 124.8, 123.7, 123.4, 122.9, 122.8, 120.7, 118.8, 52.7; ESI-MS (*m/z*) (C₃₆H₂₈N₄O₄): calcd 592.21 593 (M + H)⁺, 615 (M + Na)⁺.

Diethyl 4'-(5'-hexyl-[2,2'-bithiophen]-5-yl)-[2,2':6',2''-terpyridine]-4,4''-dicarboxylate (9c)

Yield (0.384 g, 70%) ¹H NMR (300 MHz, CDCl₃, δ in ppm): 9.17 (s, 2H), 8.8 (d, 2H), 8.6 (s, 1H), 7.9 (d, 2H), 7.6 (d, 2H), 7.2 (s, 1H), 7.14 (dd, 2H), 6.7 (s, 1H), 2.8 (q, 4H), 1.32 (m, 8H), 0.9 (t, 3H); ¹³C NMR: 165.5, 157.7, 156.3, 151.2, 146.4, 136.5, 136.2, 127.2, 126.1, 125.8, 124.6, 123.4, 123.0, 118.5, 60.7, 32.9, 31.8, 28.7, 22.7, 14.1; ESI-MS (*m/z*): calcd for (C₃₅H₃₅N₃O₄S₂), 625.21; found, 626 (M + H)⁺, 648 (M + Na)⁺.

Diethyl 4'-(10-decyl-10H-phenoxazin-3-yl)-[2,2':6',2''-terpyridine]-4,4''-dicarboxylate (9d)

Yield (0.337 g, 62%) ¹H NMR (300 MHz, CDCl₃, δ in ppm): 9.17 (s, 2H), 8.9 (d, 2H), 8.6 (s, 2H), 7.9 (d, 2H), 7.4 (d, 1H), 7.1 (s, 1H), 6.7 (t, 1H), 6.66 (t, 1H), 6.60 (d, 1H), 6.4 (m, 2H), 3.4 (t, 2H), 1.6 (m, 2H), 1.2 (m, 14H), 0.8 (q, 3H); ¹³C NMR: 165.2, 157.1, 155.0, 149.6, 148.8, 145.2, 144.6, 138.8, 134.4, 132.4, 129.7, 123.6, 122.5, 121.1, 120.7, 117.9, 115.3, 113.5, 111.4, 111.2, 61.7, 44.0, 31.8, 29.59, 29.52, 29.3, 29.2, 26.8, 24.9, 22.6, 14.21, 14.09; ESI-MS (*m/z*) calcd for (C₄₃H₄₆N₄O₅), 698.35; found, 699 (M + H)⁺, 721 (M + Na)⁺.

Diethyl 4'-(10-decyl-10H-phenothiazin-3-yl)-[2,2':6',2''-terpyridine]-4,4''-dicarboxylate (9e)

Yield (0.325 g, 60%) ¹H NMR (300 MHz, CDCl₃, δ in ppm): 9.17 (s, 2H), 8.93 (d, 2H), 8.65 (s, 2H), 7.96 (d, 2H), 7.43 (d, 2H), 7.18 (s, 1H), 6.81 (m, 1H), 6.67–6.59 (m, 3H), 6.52–6.47 (m, 2H), 4.51 (q, 4H), 3.47 (t, 2H), 1.65 (m, 2H), 1.49 (t, 6H). ¹³C NMR: 165.2, 155.3, 149.7, 138.8, 127.4, 127.3, 126.3, 125.7, 125.4, 122.8, 122.8, 122.6, 120.7, 118.4, 115.4, 61.7, 47.5, 31.8, 29.5, 29.2, 26.8, 22.6, 14.2, 14.0; ESI-MS (*m/z*) calcd for (C₄₃H₄₆N₄O₅S), 714.32; found, 715 (M + H)⁺, 737 (M + Na)⁺.

General procedure for the synthesis of [RuCl₃(4'-substituted terpyridine dicarboxylate)] (10a–10e)

Ruthenium trichloride (130 mg, 0.84 mmol) was dissolved in EtOH (30 mL), and the solution was stirred for 2 min at 50 °C. To this solution, a solution of ligand (4'-substituted terpyridine dicarboxylate, 9a–9e) (0.51 mmol) in dichloromethane (20 mL) was added, and the mixture was refluxed for 3 h. The solution was concentrated to ca. 10 mL, and then cooled to room temperature. The precipitate was filtered, washed with cold EtOH to remove unreacted ruthenium trichloride, and the product was air-dried to yield as a dark brown powder.

General procedure for the synthesis of MC113–MC117 complexes

A mixture of [RuCl₃(4'-substituted terpyridine dicarboxylate)] (0.39 mmol), aqueous ammonium thiocyanate (113 mmol) in H₂O (5 mL) in DMF (25 mL) was refluxed at 130 °C for 4 h under an argon atmosphere. Triethylamine (10 mL) and H₂O (5 mL) were then added, and the solution was refluxed for a further 24 h to hydrolyze the ester groups on the terpyridine ligand. The reaction mixture was allowed to cool, and the solvent volume was reduced on a rotary evaporator to about

5 mL. Water was added to the flux, and the insoluble solid was filtered and dried under vacuum. The isolated solid was recrystallized by methanol and diethylether. It was further purified on a Sephadex LH-20 column with 3 : 1 methanol and dichloromethane. The main band was collected and concentrated to give the corresponding ruthenium complex.

MC113: ^1H NMR (300 MHz, CDCl_3 , δ in ppm); (yield; 0.13 g, 47%) 9.1 (d, 1H), 9.0 (d, 1H), 8.7 (s, 1H), 8.6 (s, 1H), 8.3 (s, 2H), 8.1 (s, 1H), 8.0 (d, 1H), 7.85 (s, 1H), 7.6 (t, 3H), 1.42 (s, 9H). ESI-MS (m/z) calcd for 729.0; found, 729 (M^+); FT-IR (KBr) (cm^{-1}); 3418, 2958, 2108, 1715, 1602, 1543, 1483, 1398, 1323, 1292, 1233, 1164, 1112, 1007, 914, 852, 834, 787, 725, 665, 548, 455. Anal calcd for $\text{C}_{30}\text{H}_{23}\text{N}_6\text{O}_4\text{RuS}_3$, C, 48.32; H, 3.21; N, 11.24; S, 12.85. Found: C, 48.03; H, 3.12; N, 11.24; S, 12.79.

MC114: ^1H NMR (300 MHz, CDCl_3 , δ in ppm): (yield; 0.14 g, 45%) 9.04 (s, 1H), 8.2 (m, 3H), 7.7 (s, 2H), 7.7 (s, 2H), 7.56 (s, 2H), 7.4 (m, 6H), 7.2 (m, 9H). ESI-MS (m/z) calcd for 840.01, found, 840 (M^+); FT-IR (KBr) (cm^{-1}): 3422, 2924, 2767, 2103, 1719, 1586, 1541, 1513, 1488, 1463, 1407, 1366, 1327, 1283, 1199, 1173, 1108, 1007, 864, 828, 791, 757, 697, 617, 494. Anal calcd for $\text{C}_{38}\text{H}_{24}\text{N}_7\text{O}_4\text{RuS}_3$, C, 54.17; H, 2.74; N, 11.51; S, 11.17. Found C, 53.92; H, 2.94; N, 11.51; S, 10.97.

MC115: ^1H NMR (300 MHz, CDCl_3 , δ in ppm): (yield; 0.12 g, 39%) 9.1–9.0 (m, 2H), 8.4 (m, 1H), 8.2–8.1 (m, 2H), 7.6–8 (m, 4H), 7.04 (d, 2H), 6.7 (d, 1H), 2.8 (t, 2H), 1.7 (m, 2H), 1.3 (m, 6H), 0.9 (t, 3H); ESI-MS (m/z) calcd for 844.97 found, 845 (M^+); FT-IR (KBr) (cm^{-1}): 3420, 2924, 2852, 2677, 2102, 1720, 1603, 1537, 1468, 1365, 1301, 1247, 1162, 1109, 1064, 1008, 860, 797, 764, 724, 695, 440. Anal calcd for $\text{C}_{34}\text{H}_{27}\text{N}_6\text{O}_4\text{RuS}_5$, C, 48.23; H, 3.12; N, 9.63; S, 18.82. Found C, 48.09; H, 3.34; N, 9.56; S, 18.56.

MC116: ^1H NMR (300 MHz, CDCl_3 , δ in ppm): (yield; 0.14 g, 41%) 9.1–9.0 (m, 2H), 8.5–8.4 (m, 2H), 8.2–7.8 (m, 4H), 7.0–6.7 (m, 5H), 3.2 (t, 2H), 1.8 (m, 2H), 1.3 (m, 14H), 0.8 (t, 3H); ESI-MS (m/z) calcd for, 918.11; found, 918 (M^+); FT-IR (KBr) (cm^{-1}): 3422, 2923, 2851, 2679, 2105, 1721, 1589, 1524, 1494, 1466, 1371, 1273, 1164, 1111, 1009, 861, 794, 744, 561. Anal calcd for $\text{C}_{42}\text{H}_{38}\text{N}_7\text{O}_4\text{RuS}_3$, C, 54.85; H, 4.19; N, 10.54; S, 10.37. Found C, 54.72; H, 3.98; N, 10.34; S, 10.26.

MC117: ^1H NMR (300 MHz, CDCl_3 , δ in ppm): (yield; 0.15 g, 43%) 9.1–9.0 (m, 2H), 8.6–8.5 (m, 2H), 8.2–7.9 (m, 4H), 7.2–6.8 (m, 5H), 3.3 (t, 2H), 1.8 (m, 2H), 1.3 (m, 14H), 0.8 (t, 3H); ESI-MS (m/z) calcd for 934.09; found, 934 (M^+); FT-IR (KBr) (cm^{-1}): 3422, 2926, 2852, 2738, 2677, 2491, 2105, 1722, 1599, 1539, 1464, 1392, 1367, 1297, 1253, 1169, 1110, 1036, 1010, 864, 799, 749, 552, 458. Anal calcd for $\text{C}_{42}\text{H}_{38}\text{N}_7\text{O}_4\text{RuS}_4$, C, 53.88; H, 4.06; N, 10.37, S, 13.67. Found C, 53.71; H, 3.97; N, 10.26; S, 13.36.

Fabrication and characterization of DSSCs

The dye-sensitized TiO_2 electrode was prepared as follows. After cleaning, a ~ 10 μm double layer of TiO_2 particles was deposited by screen-printing on the fluorine tin oxide (FTO) coated glass (12–14 Ω per square, TEC 15, USA). Then the fabricated TiO_2 thin-film electrodes were sintered at 450 $^\circ\text{C}$ for 30 min. After that, the electrodes were immersed in acetonitrile solution (2×10^{-4} mol L^{-1} sensitizers) containing

2×10^{-3} M chenodeoxycholic acid as the coadsorbent for at least 12 h. After soaking into the dye solution, the dye-adsorbed TiO_2 working electrodes were rinsed with anhydrous acetonitrile and dried. The DSSCs used for photovoltaic measurements consists of a dye-adsorbed TiO_2 working electrode, a 45 μm thermal adhesive film (Surlyn®, USA), an organic electrolyte and a counter electrode. The Pt catalyst was deposited on the FTO glass by spraying H_2PtCl_6 solution and pyrolysis at 410 $^\circ\text{C}$ for 20 min to prepare the counter electrode. The organic electrolyte solution was a mixture of 0.5 M 1,2-dimethyl-3-propylimidazole iodide (DMPII), 0.05 M I_2 and 0.1 M LiI in acetonitrile. The active area of the TiO_2 film electrodes was 0.25 cm^2 . The DSSCs were tested under an ambient atmosphere with a 3A grade solar simulator (Newport, USA, 94043A) under AM 1.5 (100 mW cm^{-2}) illumination to obtain the photocurrent density–photovoltage (J – V) curves. The incident monochromatic photon to current conversion efficiency (IPCE) spectra were recorded as a function of wavelength from 300 to 900 nm, using a QE/IPCE measurement kit (Newport, USA). Electrochemical impedance spectroscopy (EIS) measurements were performed on a electrochemical workstation (Autolab 320, Metrohm, Switzerland) in the frequency region from 50 mHz to 1000 kHz at perturbation amplitude of 10 mV in the dark.

DFT calculations

Density functional theory (DFT) and time-dependent DFT (TDDFT) calculations were carried out to gain deeper understanding of the electronic structure and photophysical behaviour of the molecules, using the Gaussian09 program package.⁷⁰ The closed shell configurations of the five ruthenium(II) sensitizers, **MC113–MC117**, with a charge of -1 were fully optimized in the gas phase with PBE0^{71,72} hybrid functional and LANL2DZ^{73–76} basis set (double zeta quality), which uses Dunning D95V basis functions on first row atoms, Los Alamos, ECP plus DZ on Na–La, Hf–Bi, was adopted on all atoms. Vibrational frequency analysis has been carried out to ensure that there are no imaginary frequencies. Thus, the optimized structures correspond to real minima on the potential energy surface.

At the optimized geometry, TDDFT calculations were performed at the M06⁷⁷/LANL2DZ level of theory in DMF solvent by means of the Polarizable Continuum Model (PCM),^{78,79} as implemented in Gaussian09. 80 singlet–singlet excitations at S_0 optimized geometry were calculated. The software GaussSum2.2.5⁸⁰ was used to simulate the major portion of the absorption spectrum and to interpret the nature of transitions. The molecular orbital surfaces were generated by Gaussview,⁸¹ and the percentage contributions of the Ru(II) and the ligands to the respective molecular orbitals were calculated using GaussSum.

Acknowledgements

GK thanks CSIR, New Delhi for senior research fellowship. This work was financially supported by the National Basic Research Program of China under grant no. 2011CBA00700.

References

- B. O'Regan and M. Grätzel, *Nature*, 1991, **353**, 737–740.
- M. Grätzel, *Nature*, 2001, **414**, 338–344.
- M. Grätzel, *J. Photochem. Photobiol., C: Photochem. Rev.*, 2003, **2**, 145–153.
- M. K. Nazeeruddin, E. Baranoff and M. Grätzel, *Sol. Energy*, 2011, **85**, 1172–1178.
- M. Grätzel, *J. Photochem. Photobiol., A, Chem.*, 2004, **164**, 3–14.
- D. Wei, *Int. J. Mol. Sci.*, 2010, **11**, 1103–1113.
- A. S. Polo, M. K. Itokazu and N. Y. M. Iha, *Coord. Chem. Rev.*, 2004, **248**, 1343–1361.
- M. K. Nazeeruddin, S. M. Zakeeruddin, R. H. Baker, M. Jirousek, P. Lisk, N. Vlachopoulos, V. Shklover, C.-H. Fischer and M. Grätzel, *Inorg. Chem.*, 1999, **38**, 6298–6305.
- M. K. Nazeeruddin, R. Splivallo, P. Liska, P. Comte and M. Grätzel, *Chem. Commun.*, 2003, 1456–1457.
- M. K. Nazeeruddin and P. Pechy, *Chem. Commun.*, 1997, 1705–1706.
- M. K. Nazeeruddin, F. D. Angelis, S. Fantacci, A. Selloni, G. Viscardi and P. Liska, *J. Am. Chem. Soc.*, 2005, **127**, 16835–16847.
- M. K. Nazeeruddin, A. Kay, I. Rodicio, R. Humphry-Baker, E. Mueller, P. Liska, N. Vlachopoulos and M. Grätzel, *J. Am. Chem. Soc.*, 1993, **115**, 6382–6390.
- M. K. Nazeeruddin, P. Pechy, T. Renouard, S. M. Zakeeruddin, R. Humphry-Baker, P. Comte, P. Liska, L. Cevey, E. Costa, V. Shklover, L. Spiccia, G. B. Deacon, C. A. Bignozzi and M. Grätzel, *J. Am. Chem. Soc.*, 2001, **123**, 1613–1624.
- S. R. Jang, C. C. Lee, H. B. Choi, J. J. Ko, J. Lee, R. Vittal and K. J. Kim, *Chem. Mater.*, 2006, **18**, 5604–5608.
- P. G. Bomben, K. C. D. Robson, B. D. Koivisto and C. P. Berlinguett, *Coord. Chem. Rev.*, 2012, **256**, 1438–1450.
- B. Liu, W. Zhu, W. Wu, K. M. Ri and H. Tian, *J. Photochem. Photobiol., A: Chem.*, 2008, **194**, 268–274.
- S. A. Haque, S. Handa, K. Peter, E. Palomares, M. Thelakkat and J. R. Durrant, *Angew. Chem., Int. Ed.*, 2005, **44**, 5740–5744.
- M. J. Scott, J. J. Nelson, S. Caramori, C. A. Bignozzi and C. M. Elliott, *Inorg. Chem.*, 2007, **46**, 10071–10078.
- D. Kuciauskas, M. S. Freund, H. B. Gray, J. R. Winkler and N. S. Lewis, *J. Phys. Chem. B*, 2001, **105**, 392–403.
- R. Argazzi, G. Larramona, C. Contado and C. A. Bignozzi, *J. Photochem. Photobiol., A: Chem.*, 2004, **164**, 15–21.
- S. Ferrere and B. A. Gregg, *J. Am. Chem. Soc.*, 1998, **120**, 843–844.
- J. E. Monat and J. K. McCusker, *J. Am. Chem. Soc.*, 2000, **122**, 4092–4097.
- L. Schmidt-Mende, U. Bach, R. Humphry-Baker, T. Horiuchi, H. Miura, S. Ito, S. Uchida and M. Grätzel, *Adv. Mater.*, 2005, **17**, 813–815.
- Y.-S. Yen, H.-H. Chou, Y.-C. Chen, C.-Y. Hsu and J. T. Lin, *J. Mater. Chem.*, 2012, **22**, 8734–8747.
- W. H. Howie, F. Claeysens, H. Miura and L. M. Peter, *J. Am. Chem. Soc.*, 2008, **130**, 1367–1375.
- M. Mao, J.-B. Wang, Z.-F. Xiao, S.-Y. Dai and Q.-H. Song, *Dyes Pigm.*, 2012, **94**, 224–232.
- G. Marotta, M. A. Reddy, S. P. Singh, A. Islam, L. Han, F.-D. Angelis, M. Pastore and M. Chandrasekharam, *ACS Appl. Mater. Interfaces*, 2013, **5**, 9635–9647.
- K. S. V. Gupta, T. Suresh, S. P. Singh, A. Islam, L. Han and M. Chandrasekharam, *Org. Electron.*, 2014, **15**, 266–275.
- W. M. Campbell, K. W. Jolley, P. Wagner, K. Wagner, P. J. Walsh, K. C. Gordon, L. S. Mende, M. K. Nazeeruddin, Q. Wang, M. Grätzel and D. L. Officer, *J. Phys. Chem. C*, 2007, **111**, 11760–11762.
- A. Yella, H.-W. Lee, H. N. Tsao, C. Yi, A. K. Chandiran, M. K. Nazeeruddin, E. W.-G. Diau, C.-Y. Yeh, S. M. Zakeeruddin and M. Grätzel, *Science*, 2011, **334**, 629–633.
- Z. Jin, H. Masuda, N. Yamanaka, M. Minami, T. Nakamura and Y. Nishikitani, *Chem. Lett.*, 2009, **38**, 44.
- P. A. Anderson, G. F. Strouse, J. A. Treadway, F. R. Keene and T. J. Meyer, *Inorg. Chem.*, 1994, **33**, 3863–3864.
- P. Wang, S. M. Zakeeruddin, J.-E. Moser, R. Humphry-Baker, P. Comte, V. Aranyos, A. Hagfeldt, M. K. Nazeeruddin and M. Grätzel, *Adv. Mater.*, 2004, **16**, 1806–1811.
- Y. Cao, Y. Bai, Q. Yu, Y. Cheng, S. Liu, D. Shi, F. Gao and P. Wang, *J. Phys. Chem. C*, 2009, **113**, 6290–6297.
- C.-Y. Chen, S.-J. Wu, J.-Y. Li, C.-G. Wu, J.-G. Chen and K.-C. Ho, *Adv. Mater.*, 2007, **19**, 3888–3891.
- M. G. Lobello, K.-L. Wu, M. A. Reddy, G. Marotta, M. Grätzel, M. K. Nazeeruddin, Y. Chi, M. Chandrasekharam, G. Vitillarova and F. D. Angelis, *Dalton Trans.*, 2014, **43**, 2726–2732.
- M. Chandrasekharam, M. A. Reddy, S. P. Singh, B. Priyanka, K. Bhanuprakash, M. Lakshmi Kantam, A. Islam and L. Han, *J. Mater. Chem.*, 2012, **22**, 18757–18760.
- M. Chandrasekharam, T. Suresh, S. P. Singh, B. Priyanka, K. Bhanuprakash, A. Islam, L. Han and M. Lakshmi Kantam, *Dalton Trans.*, 2012, **41**, 8770–8772.
- T. Suresh, G. Rajkumar, S. P. Singh, P. Y. Reddy, A. Islam, L. Han and M. Chandrasekharam, *Org. Electron.*, 2013, **14**, 2243–2248.
- T. Suresh, K. Ganesh, S. P. Singh, A. Islam, L. Han and M. Chandrasekharam, *Dyes Pigm.*, 2013, **99**, 850–856.
- M. Chandrasekharam, G. Rajkumar, Ch. Srinivasa Rao, T. Suresh, P. Y. Reddy, J.-H. Yum, M. K. Nazeeruddin and M. Grätzel, *J. Nanosci. Nanotechnol.*, 2011, **2**(035016), 1–15.
- M. Chandrasekharam, G. Rajkumar, T. Suresh, Ch. Srinivasa Rao, P. Y. Reddy, J.-H. Yum, M. K. Nazeeruddin and M. Grätzel, *Adv. Opto. Electron.*, 2011, **963068**, 1–10.
- S.-H. Yang, K.-L. Wu, Y. Chi, Yi-M. Cheng and Pi-T. Chou, *Angew. Chem., Int. Ed.*, 2011, **50**, 8270–8274.

- 44 K.-L. Wu, C.-H. Li, Y. Chi, J. N. Clifford, L. Cabau, E. Palomares, Yi-M. Cheng, H.-A. Pan and Pi-T. Chou, *J. Am. Chem. Soc.*, 2012, **134**, 7488–7496.
- 45 Y. Numata, S. P. Singh, A. Islam, M. Iwamura, A. Imai, K. Nozaki and L. Han, *Adv. Funct. Mater.*, 2013, **23**, 1817–1823.
- 46 L. Han, A. Islam, H. Chen, M. Chandrasekharan, B. Chiranjeevi, S. Zhang, X. Yang and M. Yanagida, *Energy Environ. Sci.*, 2012, **5**, 6057–6060.
- 47 M. Chandrasekharan, G. Rajkumar, Ch. Srinivasarao, T. Suresh, P. Y. Reddy and Y. Soujanya, *J. Chem. Sci.*, 2011, **123**, 555–565.
- 48 K. Cao, J. Lu, J. Cui, Y. Shen, W. Chen, G. Alemu, Z. Wang, H. Yuan, J. Xu, M. Wang and Y. Cheng, *J. Mater. Chem. A*, 2014, **2**, 4945–4953.
- 49 K. C. D. Robson, B. D. Koivisto, T. J. Gordon, T. Baumgartner and C. P. Berlinguette, *Inorg. Chem.*, 2010, **49**(12), 5335–5337.
- 50 C.-Y. Chen, S.-J. Wu, C.-G. Wu, J.-G. Chen and K.-C. Ho, *Angew. Chem., Int. Ed.*, 2006, **45**, 5822–5825.
- 51 M. Chandrasekharan, G. Rajkumar, T. Suresh and P. Y. Reddy, *Adv. Opto. Electron.*, 2012, **482074**, 1–10.
- 52 X. Kong, A. P. Kulkarni and S. A. Jenekhe, *Macromolecules*, 2003, **36**, 8992–8999.
- 53 M. Chandrasekharan, G. Rajkumar, Ch. SrinivasaRao, T. Suresh and P. Y. Reddy, *Synth. Met.*, 2011, **161**, 1469–1476.
- 54 H. Tian, X. Yang, J. Cong, R. Chen, J. Liu, Y. Hao, A. Hagfeldt and L. Sun, *Chem. Commun.*, 2009, 6288–6290.
- 55 S. Agrawal, M. Pastore, G. Marotta, M. A. Reddy, M. Chandrasekharan and F. D. Angelis, *J. Phys. Chem. C*, 2013, **117**, 9613–9622.
- 56 F. Kröhnke, *Synthesis*, 1976, 1.
- 57 P. C. Andrews, G. B. Deacon, R. Frank, B. H. Fraser, P. C. Junk, J. G. MacLellan, M. Massi, B. Moubaraki, K. S. Murray and M. Silberstein, *Eur. J. Inorg. Chem.*, 2009, 744–751.
- 58 J. Dehaut, J. Husson and L. Guyard, *Green Chem.*, 2011, **13**, 3337–3340.
- 59 Q. Wang, J. E. Moser and M. Grätzel, *J. Phys. Chem. B*, 2005, **109**, 14945–14953.
- 60 A. Burke, S. Ito, H. Snaith, U. Bach, K. Kwiatkowski and M. Grätzel, *Nano Lett.*, 2008, **8**, 977–1270.
- 61 Z. J. Ning, Q. Zhang, H. C. Pei, J. F. Luan, C. G. Lu, Y. P. Cui and H. Tian, *J. Phys. Chem. C*, 2009, **113**, 10307–10313.
- 62 Y. Ooyama and Y. Harima, *Eur. J. Org. Chem.*, 2009, 2903–2934.
- 63 C. Klein, M. K. Nazeeruddin, D. D. Censo, P. Liska and M. Grätzel, *Inorg. Chem.*, 2004, **43**, 4216–4226.
- 64 Y. J. Chang and T. J. Chow, *Tetrahedron*, 2009, **65**, 9626–9632.
- 65 S. Hwang, J. H. Lee, C. Park, H. Lee, C. Kim, M. H. Lee, W. Lee, J. Park, K. Kim and N. G. Park, *Chem. Commun.*, 2007, 4887–4889.
- 66 R. Z. Li, D. Shi, D. F. Zhou, Y. M. Cheng, G. L. Zhang and P. Wang, *J. Phys. Chem. C*, 2009, **113**, 7469–7479.
- 67 W. Wu, J. Yang, J. Hua, J. Tang, L. Zhang, Y. Long and H. Tian, *J. Mater. Chem.*, 2010, **20**, 1772–1779.
- 68 S. Ito, S. M. Zakeeruddin, R. H. Baker, P. Liska, R. Charvet, P. Comte, M. K. Nazeeruddin, P. Pechy, M. Takata, H. Miura, S. Uchida and M. Grätzel, *Adv. Mater.*, 2006, **18**, 1202–1205.
- 69 K. Hara, T. Sato, R. Katoh, A. Furube, Y. Ohga, A. Shinpo, S. Suga, K. Sayama, H. Sugihara and H. Arakawa, *J. Phys. Chem. B*, 2003, **107**, 597–606.
- 70 M. J. Frisch, G. W. Trucks, H. B. Schlegel, G. E. Scuseria, M. A. Robb, J. R. Cheeseman, G. Scalmani, V. Barone, B. Mennucci and G. A. Petersson, *et al.*, *Gaussian 09, Revision B.01*, Gaussian, Inc., Wallingford, CT, 2010.
- 71 J. P. Perdew, K. Burke and M. Ernzerhof, *Phys. Rev. Lett.*, 1996, **77**, 3865–3868.
- 72 J. P. Perdew, K. Burke and M. Ernzerhof, *Phys. Rev. Lett.*, 1997, **78**, 1396–1396.
- 73 T. H. Dunning and P. J. Hay, *Methods of Electronic Structure Theory*, ed. H. F. Schaefer III, *Modern Theoretical Chemistry*, Plenum, New York, 1976, vol. 3, pp. 1–28.
- 74 P. J. Hay and W. R. Wadt, *J. Chem. Phys.*, 1985, **82**, 270–283.
- 75 W. R. Wadt and P. J. Hay, *J. Chem. Phys.*, 1985, **82**, 284–298.
- 76 P. J. Hay and W. R. Wadt, *J. Chem. Phys.*, 1985, **82**, 299–310.
- 77 Y. Zhao and D. G. Truhlar, *Theor. Chem. Acc.*, 2008, **120**, 215–224.
- 78 S. Miertuš, E. Scrocco and J. Tomasi, *Chem. Phys.*, 1981, **55**, 117–129.
- 79 M. Cossi, V. Barone, R. Cammi and J. Tomasi, *J. Chem. Phys. Lett.*, 1996, **255**, 327–335.
- 80 N. M. O’Boyle, A. L. Tenderholt and K. M. Langner Igorithms, *J. Comput. Chem.*, 2008, **29**, 839–845.
- 81 R. Dennington, T. Keith and J. Millam, *GaussView, Version 5*, Semichem Inc., ShawneeMissionKS, 2009.